Unsteady motion of a long bubble or droplet in a self-rewetting system

B. R. Duffy,[1,*] S. K. Wilson,[1,†] J. J. A. Conn,[1] and K. Sefiane[2,‡]
[1]*Department of Mathematics and Statistics, University of Strathclyde, Livingstone Tower, 26 Richmond Street, Glasgow G1 1XH, United Kingdom*
[2]*School of Engineering, University of Edinburgh, The King's Buildings, Mayfield Road, Edinburgh EH9 3FB, United Kingdom*

(Received 17 August 2018; published 17 December 2018)

Motivated by the potential use of self-rewetting fluids (i.e., fluids that exhibit a nonmonotonic variation of surface tension with temperature) in various heat-transfer applications, in the present work we formulate and analyze a theoretical model for the unsteady motion of a long bubble or droplet in a self-rewetting system in a nonuniformly heated tube due to a combination of Marangoni effects due to the variation of surface tension with temperature, gravitational effects due to the density difference between the two fluids, and an imposed background flow along the tube. We find that the evolution of the shape (but not of the position) of the bubble or droplet is driven entirely by Marangoni effects and depends on the initial value of its radius in relation to a critical value. In the case in which Marangoni effects are absent, the bubble or droplet always moves with constant velocity without changing shape. In the case in which only Marangoni effects are present, the bubble or droplet either always moves away from or always moves towards the position of minimum surface tension; in the latter case it ultimately fills the entire cross section of the tube at a final stationary position which is closer to the position of minimum surface tension than its original position. In the cases in which either only Marangoni effects and gravitational effects or only Marangoni effects and background-flow effects are present the competition between the two effects can lead to a nonmonotonic evolution of the position of the center of mass of the bubble or droplet. The behavior of a self-rewetting system described in the present work is qualitatively different from that for ordinary fluids, in which case the bubble or droplet always moves with constant velocity without changing shape.

DOI: 10.1103/PhysRevFluids.3.123603

I. INTRODUCTION

The thermocapillary-driven (i.e., surface-tension-gradient-driven, hereafter referred to simply as "Marangoni-driven") motion of bubbles and droplets plays an important role in a wide variety of practical situations including, for example, heat-transfer and material-processing applications. For most "ordinary" fluids, surface tension, here denoted by σ, is a monotonically (typically, to a good approximation, linearly) decreasing function of temperature, here denoted by T [see, for example, Fig. 1(a)], and as a result Marangoni effects draw fluid towards regions with lower temperature. However, for many years it has been known (see, for example, the pioneering work of Vochten and Petre [1], Petre and Azouni [2], Legros [3], and Vázquez, Alvarez, and Navaza [4]) that this behavior is not universal, and that there are certain fluids, notably dilute aqueous solutions of

*b.r.duffy@strath.ac.uk
†Corresponding author: s.k.wilson@strath.ac.uk
‡k.sefiane@ed.ac.uk

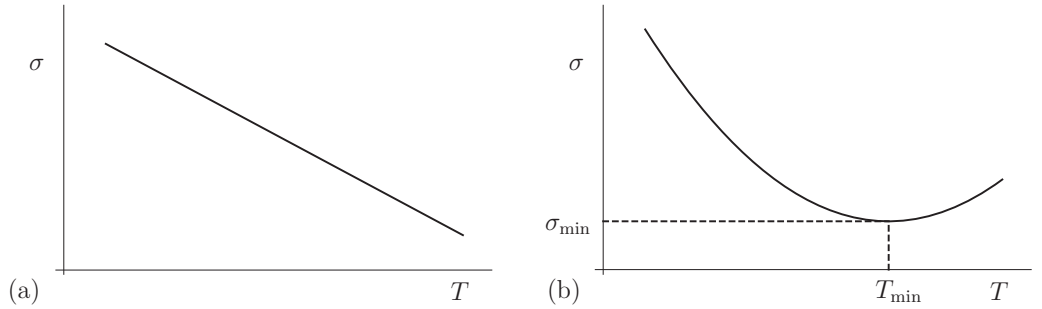

FIG. 1. Sketches of surface tension σ as a function of temperature T for (a) an ordinary and (b) a self-rewetting fluid.

certain long-chain alcohols, that exhibit a nonmonotonic (typically, to a good approximation, locally quadratic) variation of surface tension with temperature, with a minimum value, here denoted by $\sigma_{\min}$, at a well-defined value of temperature, here denoted by $T_{\min}$ [see, for example, Fig. 1(b)]. In particular, for temperatures above $T_{\min}$ the surface tension of such fluids is an increasing function of temperature, and as a result Marangoni effects draw fluid towards regions with higher temperature. This unusual behavior has stimulated interest in the potential use of such fluids in various heat-transfer applications, such as pool boiling, spray boiling, and heat pipes, because in these contexts it tends to reduce dry-out, and hence to enhance the overall heat transfer, by rewetting hot surfaces, and so has led to them being termed "self-rewetting" fluids (see, for example, the work of Zhang [5], Abe, Iwasaki and Tanaka [6,7], Abe [8], Savino and collaborators [9–15], Hu *et al.* [16], Hu, Zhang, and Wang [17], and Wu [18]).

There have been a few studies of the effect of a nonmonotonic variation of surface tension with temperature on the dynamics of fluid films (notably the early work by Oron and Rosenau [19], Slavtchev and Miladinova [20], and the more recent work by Batson, Agnon, and Oron [21]). However, in contrast to the large body of work on the motion of both confined and unconfined bubbles and droplets in or of an ordinary fluid in the presence of significant Marangoni effects (see, for example, the work of Young, Goldstein, and Block [22], Balasubramaniam and Chai [23], Ehrhard and Davis [24], Wilson [25,26], Smith [27], Balasubramaniam and Subramanian [28], Mazouchi and Homsy [29,30], Lajeunesse and Homsy [31], Dunn *et al.* [32], Katz *et al.* [33], and Karapetsas, Sahu, and Matar [34]), until recently there has been virtually no work on the motion of a bubble or droplet in or of a self-rewetting fluid. These studies show that the behavior of a bubble or droplet in or of a self-rewetting fluid can be qualitatively different from that for an ordinary fluid. Specifically, the theoretical studies by Karapetsas *et al.* [35] of the motion of a droplet on a heated substrate, and by Tripathi *et al.* [36] of the rise of a bubble in a vertical channel, as well as the experimental studies by Shanahan and Sefiane [37] of the motion of a bubble in a mean flow, and by Mamalis, Koutsos, and Sefiane of the motion of a droplet on a heated inclined substrate [38], of the rise of a bubble in a vertical micro-channel [39], and of the spreading of a droplet on a heated substrate [40], all demonstrate this. In the present work we seek to bring further insight into this problem by formulating and analyzing a theoretical model for the unsteady motion of a long bubble or droplet in a self-rewetting system in a nonuniformly heated tube. In particular, we find that the evolution of the shape (but not of the position) of the bubble or droplet is driven entirely by Marangoni effects and depends on the initial value of its radius in relation to a critical value.

II. PROBLEM FORMULATION

Consider the unsteady motion of a long axisymmetric bubble or droplet of fluid (denoted fluid 1), with constant volume V, uniform radius $b(t)$, and length $L(t)$, where t denotes time, in a second fluid (denoted fluid 2), all contained within a nonuniformly heated vertical tube of constant radius

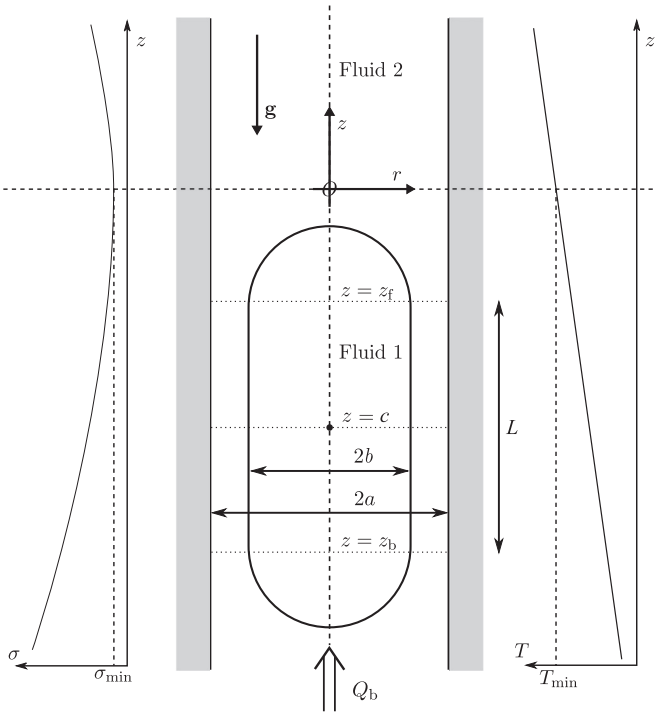

FIG. 2. Sketch of the geometry of the problem: a long axisymmetric bubble or droplet of fluid (fluid 1) of uniform radius $b(t)$ moving in a second fluid (fluid 2), all contained within a nonuniformly heated vertical tube of constant radius a. The linear temperature distribution T imposed on the tube wall and the resulting quadratic variation of surface tension σ are shown on the right and the left of the figure, respectively.

a, where $0 < b(t) < a \ll L(t)$. The motion is due to a combination of Marangoni effects due to the variation of surface tension with temperature, gravitational effects due to the density difference between the two fluids, and an imposed background flow along the tube with prescribed axial volume flux Q_b. For brevity, henceforth we use the general term "droplet" rather than "bubble or droplet," except when explicitly referring to the special case in which fluid 1 is inviscid.

Figure 2 shows a sketch of the geometry of the problem. We choose a cylindrical polar coordinate system, with the z axis vertically upwards along the centerline of the tube, and with the origin $z = 0$ at the vertical position at which the wall temperature takes the value T_min. With respect to this coordinate system, the velocity, pressure, and temperature of fluid i for $i = 1, 2$ are denoted by $\mathbf{u}_i = (u_i, w_i)$, $p_i(r, z, t)$, and $T_i(r, z, t)$, respectively, where $u_i(r, z, t)$ and $w_i(r, z, t)$ denote the radial and the axial velocity, respectively. The positions of the front and back of the droplet are denoted by $z = z_\mathrm{f}(t)$ and $z = z_\mathrm{b}(t) = z_\mathrm{f}(t) - L(t)\,(< z_\mathrm{f}(t))$, respectively, in terms of which the position of the center of mass of the droplet is given by $z = c(t) = (z_\mathrm{f}(t) + z_\mathrm{b}(t))/2$.

We assume that both fluids are incompressible, with constant bulk material properties which may differ between the two fluids. Specifically, fluid i for $i = 1, 2$ has constant density ρ_i, dynamic viscosity μ_i, heat capacity $c_{\mathrm{p},i}$, and thermal conductivity k_i.

To model the self-rewetting properties of the system we take the surface tension of the interface between the two fluids, σ, to be a quadratic function of temperature T with a minimum value $\sigma = \sigma_\mathrm{min}$ at $T = T_\mathrm{min}$ given by

$$\sigma = \sigma_\mathrm{min} + \frac{\gamma}{2}(T - T_\mathrm{min})^2, \tag{1}$$

where $\gamma = d^2\sigma/dT^2 > 0$ is a positive constant.

A linear temperature distribution is imposed on the tube wall, and so

$$T_2 = T_{\min} + \beta z \quad \text{on } r = a, \tag{2}$$

where the constant β is the imposed temperature gradient, which may be positive or negative depending on whether the top or the bottom of the tube is hotter. However, since σ is a quadratic function of $T - T_{\min}$, we find that it depends on β like β^2 (rather than like β, as it would do for ordinary fluids for which σ is a linearly decreasing function of T), and therefore we may, without loss of generality, take β to be positive (i.e., we may, without loss of generality, consider the situation shown in Fig. 2 in which the top of the tube is hotter than the bottom).

Since the droplet is long compared with the radius of the tube, its aspect ratio ε, defined by

$$\varepsilon = \frac{a}{\ell} \ll 1, \tag{3}$$

is small, where

$$\ell = \frac{V}{\pi a^2} \tag{4}$$

is a characteristic axial length scale of the problem, chosen such that the scaled volume of the droplet is unity. It is then appropriate to nondimensionalize and scale all relevant quantities in the system according to

$$\left.\begin{gathered} r^* = \frac{r}{a}, \quad b^* = \frac{b}{a}, \quad z^* = \frac{\varepsilon z}{a}, \quad L^* = \frac{\varepsilon L}{a}, \quad t^* = \frac{\varepsilon W t}{a}, \quad u_i^* = \frac{u_i}{\varepsilon W}, \quad w_i^* = \frac{w_i}{W}, \\ p_i^* = \frac{\varepsilon a p_i}{\mu_2 W}, \quad Q_i^* = \frac{Q_i}{\pi a^2 W}, \quad Q_{\mathrm{b}}^* = \frac{Q_{\mathrm{b}}}{\pi a^2 W}, \quad T_i^* = \frac{T_i - T_{\min}}{T_{\min}}, \quad \beta^* = \frac{a\beta}{\varepsilon T_{\min}}, \quad \sigma^* = \frac{\sigma}{\sigma_{\min}}, \end{gathered}\right\} \tag{5}$$

where the stars denote dimensionless quantities, Q_i^* for $i = 1, 2$ denote the axial volume fluxes of fluid 1 and fluid 2, respectively, given by

$$Q_1^* = 2\int_0^{b^*} r^* w_1^*\, dr^*, \quad Q_2^* = 2\int_{b^*}^1 r^* w_2^*\, dr^*, \tag{6}$$

and W is the characteristic axial velocity scale. The particular form for W may be chosen in several different ways, such as $W = \varepsilon\gamma T_{\min}^2/\mu_2$ when Marangoni effects are important, $W = (\rho_2 - \rho_1)ga^2/\mu_2$ when gravitational effects are important, or $W = Q_{\mathrm{b}}/\pi a^2$ when the background-flow effects are important, and so we leave W unspecified here.

Away from the ends of the droplet and at leading order in the limit $\varepsilon \to 0$, the velocity, pressure, and temperature of the two fluids satisfy

$$\frac{1}{r^*}\frac{\partial}{\partial r^*}(r^* u_1^*) + \frac{\partial w_1^*}{\partial z^*} = 0, \quad \frac{1}{r^*}\frac{\partial}{\partial r^*}(r^* u_2^*) + \frac{\partial w_2^*}{\partial z^*} = 0, \tag{7}$$

$$\frac{\partial p_1^*}{\partial r^*} = 0, \quad \frac{\partial p_2^*}{\partial r^*} = 0, \tag{8}$$

$$\frac{m}{r^*}\frac{\partial}{\partial r^*}\left(r^*\frac{\partial w_1^*}{\partial r^*}\right) = \frac{\partial p_1^*}{\partial z^*} + \rho_1^*, \quad \frac{1}{r^*}\frac{\partial}{\partial r^*}\left(r^*\frac{\partial w_2^*}{\partial r^*}\right) = \frac{\partial p_2^*}{\partial z^*} + \rho_2^*, \tag{9}$$

$$\frac{1}{r^*}\frac{\partial}{\partial r^*}\left(r^*\frac{\partial T_1^*}{\partial r^*}\right) = 0, \quad \frac{1}{r^*}\frac{\partial}{\partial r^*}\left(r^*\frac{\partial T_2^*}{\partial r^*}\right) = 0, \tag{10}$$

representing balances of mass, linear momentum in the radial direction, linear momentum in the axial direction, and energy, respectively, and where we have assumed that the reduced Reynolds numbers $\varepsilon^2\mathrm{Re}_i$ and the reduced Péclet numbers $\varepsilon^2\mathrm{Pe}_i$ for $i = 1, 2$, defined by

$$\varepsilon^2\mathrm{Re}_i = \frac{\varepsilon\rho_i a W}{\mu_i} \ll 1, \quad \varepsilon^2\mathrm{Pe}_i = \frac{\varepsilon\rho_i c_{\mathrm{p},i} a W}{k_i} \ll 1, \tag{11}$$

in both fluids are small, and have defined the viscosity ratio,

$$m = \frac{\mu_1}{\mu_2}, \tag{12}$$

along with the scaled densities of fluid 1 and fluid 2, respectively,

$$\rho_1^* = \frac{\rho_1 g a^2}{\mu_2 W}, \quad \rho_2^* = \frac{\rho_2 g a^2}{\mu_2 W}, \tag{13}$$

and the scaled density difference between the two fluids,

$$\Delta\rho^* = \frac{(\rho_2 - \rho_1) g a^2}{\mu_2 W}. \tag{14}$$

The special cases of an inviscid bubble and of an inviscid surrounding fluid correspond to $m = 0$ and the limit $m \to \infty$, respectively.

Equations (7)–(10) are subject to the following leading-order boundary conditions. At the axis of symmetry, $r^* = 0$,

$$u_1^* = 0, \tag{15}$$

$$\frac{\partial w_1^*}{\partial r^*} = 0, \tag{16}$$

$$\frac{\partial T_1^*}{\partial r^*} = 0. \tag{17}$$

At the tube wall, $r^* = 1$,

$$u_2^* = 0, \tag{18}$$

$$w_2^* = 0, \tag{19}$$

$$T_2^* = \beta^* z^*, \tag{20}$$

which are a no-penetration condition, a no-slip condition, and the imposed wall temperature, respectively. At the interface between the two fluids, $r^* = b^*$,

$$u_1^* = u_2^*, \tag{21}$$

$$w_1^* = w_2^*, \tag{22}$$

$$T_1^* = T_2^*, \tag{23}$$

$$\kappa \frac{\partial T_1^*}{\partial r^*} = \frac{\partial T_2^*}{\partial r^*}, \tag{24}$$

$$p_1^* - p_2^* = \frac{1}{b^*}\left(\frac{1}{C} + \frac{M}{2\beta^2} T_1^{*2}\right), \tag{25}$$

$$\frac{\partial w_2^*}{\partial r^*} - m \frac{\partial w_1^*}{\partial r^*} = -\frac{M}{\beta^2} T_1^* \frac{\partial T_1^*}{\partial z^*}, \tag{26}$$

which are continuity of radial velocity, axial velocity, temperature and heat flux, and balances of normal stresses and tangential stresses, respectively, where we have defined the thermal conductivity ratio,

$$\kappa = \frac{k_1}{k_2}, \tag{27}$$

an appropriate capillary number,

$$C = \frac{\mu_2 W}{\varepsilon \sigma_{\min}}, \tag{28}$$

and an appropriate Marangoni number,

$$M = \frac{\varepsilon \gamma \beta^2 T_{\min}^2}{\mu_2 W}. \tag{29}$$

Global conservation of mass requires that the total flux of the two fluids must be equal to the prescribed flux of the imposed background flow, Q_{b}^*, i.e.,

$$Q_1^* + Q_2^* = Q_{\mathrm{b}}^*. \tag{30}$$

In particular, in the special case of a closed tube with no background flow, $Q_{\mathrm{b}}^* = 0$, and so $Q_1^* = -Q_2^*$.

Note that, whereas $\Delta\rho^*$ and Q_{b}^* may be either positive, negative, or zero, M must, by definition, always be non-negative.

The radius of the droplet, b^*, satisfies the kinematic condition

$$2b^* \frac{db^*}{dt^*} + \frac{\partial Q_1^*}{\partial z^*} = 0, \quad \text{or, equivalently,} \quad 2b^* \frac{db^*}{dt^*} - \frac{\partial Q_2^*}{\partial z^*} = 0. \tag{31}$$

Neglecting the small contributions from its ends, the volume of the droplet is given by $b^{*2} L^* = 1$, and hence its length is simply given by

$$L^* = \frac{1}{b^{*2}}. \tag{32}$$

Note that, since the (dimensional) radius of the droplet must be less than that of the tube (i.e., $0 < b < a$ and hence $0 < b^* < 1$), its (dimensional) length must be greater than the characteristic axial length scale ℓ given by Eq. (4) (i.e., $L > \ell$ and hence $L^* > 1$). Henceforth, for clarity, we drop the stars on dimensionless quantities.

III. PROBLEM SOLUTION

The thermal problem, given by Eqs. (10), (17), (20), (23), and (24), decouples from the hydrodynamic problem and may be solved separately to yield simply

$$T_1 = T_2 = \beta z, \tag{33}$$

showing that the temperatures of both fluids are radially uniform and identically equal to the imposed wall temperature. In particular, this means that the surface tension given by Eq. (1) is a quadratic function of z given by

$$\sigma = 1 + \frac{MC}{2} z^2. \tag{34}$$

The hydrodynamic problem, given by Eqs. (7)–(9), (15), (16), (18), (19), (21), (22), (25), and (26), may now be solved, leading ultimately to the evolution equations for the shape of the droplet and for its position within the tube [i.e., evolution equations for $b(t)$, $L(t)$, $z_{\mathrm{f}}(t)$, $z_{\mathrm{b}}(t)$ and $c(t)$].

Equation (8) implies that the pressures of both fluids are radially uniform, i.e.,

$$p_i = p_i(z, t) \quad \text{for} \quad i = 1, 2. \tag{35}$$

In particular, using Eqs. (33) and (35), Eq. (25) shows that

$$p_1 - p_2 = \frac{1}{b}\left(\frac{1}{C} + \frac{M}{2} z^2\right). \tag{36}$$

Using Eq. (35), Eq. (9) may be integrated to yield expressions for the axial velocities w_i, which may then be used to determine the radial velocities u_i and fluxes Q_i of both fluids. The expressions for the pressure gradients and the velocities of both fluids are rather cumbersome, and therefore have been relegated to Appendix A. However, the fluxes take the forms

$$Q_1 = Mzf_{\mathrm{M}}(b,m) + \Delta\rho f_{\mathrm{G}}(b,m) + Q_{\mathrm{b}} f_{\mathrm{B}}(b,m), \quad Q_2 = Q_{\mathrm{b}} - Q_1, \tag{37}$$

where the functions f_j for $j = \mathrm{M}, \mathrm{G}, \mathrm{B}$, which arise in the Marangoni (M), gravitational (G), and background-flow (B) contributions to the fluxes, are given by

$$f_{\mathrm{M}}(b,m) = \frac{b^3}{8}\left[\frac{(1-b^2)[(4m-1)b^2-4m-1]}{m-(m-1)b^4} - 4\ln b\right], \tag{38}$$

$$f_{\mathrm{G}}(b,m) = \frac{b^4}{8}\left[\frac{(1-b^2)[(4m-3)b^2-4m+1]}{m-(m-1)b^4} - 4\ln b\right] \quad (>0), \tag{39}$$

$$f_{\mathrm{B}}(b,m) = \frac{b^2[2m-(2m-1)b^2]}{m-(m-1)b^4} \quad (>0), \tag{40}$$

respectively.

Figure 3 shows f_j for $j = \mathrm{M}, \mathrm{G}, \mathrm{B}$ plotted as functions of b for the full range of values of m. Each of the f_j varies monotonically with m, with f_{M} increasing but f_{G} and f_{B} decreasing as m increases. In particular, in the special case of an inviscid bubble ($m = 0$), Eqs. (38)–(40) reduce to

$$f_{\mathrm{M}}(b,0) = -\frac{1-b^4}{8b} - \frac{b^3}{2}\ln b \quad (<0), \tag{41}$$

$$f_{\mathrm{G}}(b,0) = \frac{(1-b^2)(1-3b^2)}{8} - \frac{b^4}{2}\ln b \quad (>0), \tag{42}$$

$$f_{\mathrm{B}}(b,0) = 1, \tag{43}$$

while in the special case of an inviscid surrounding fluid ($m \to \infty$), Eqs. (38)–(40) reduce to

$$f_{\mathrm{M}}(b,\infty) = -\frac{b^3}{2}\left(\frac{1-b^2}{1+b^2} + \ln b\right) \quad (>0), \tag{44}$$

$$f_{\mathrm{G}}(b,\infty) = -\frac{b^4}{2}\left(\frac{1-b^2}{1+b^2} + \ln b\right) = b f_{\mathrm{M}}(b,\infty) \quad (>0), \tag{45}$$

$$f_{\mathrm{B}}(b,\infty) = \frac{2b^2}{1+b^2} \quad (>0), \tag{46}$$

respectively. In addition, we note that $f_{\mathrm{M}} = -(1/2)b^3\ln b + O(b^3) \to 0^+$, $f_{\mathrm{G}} = -(1/2)b^4\ln b + O(b^4) \to 0^+$, and $f_{\mathrm{B}} = 2b^2 + O(b^4) \to 0^+$ in the limit $b \to 0^+$, and that $f_{\mathrm{M}} = -(1-b)^2 + O((1-b)^3) \to 0^-$, $f_{\mathrm{G}} = (2/3)(1-b)^3 + O((1-b)^4) \to 0^+$, and $f_{\mathrm{B}} = 1 - 4m(1-b)^2 + O((1-b)^3) \to 1^-$ in the limit $b \to 1^-$.

As Fig. 3 shows, the functions f_{G} and f_{B} are always positive, meaning that, as expected, the contributions to Q_1 and $-Q_2$ due to gravitational and background-flow effects are always of the same sign as $\Delta\rho$ and Q_{b}, respectively, but the function f_{M} can be either positive, negative, or zero, and so, despite the fact that M is always non-negative, the contribution to Q_1 and $-Q_2$ due to Marangoni effects may be either positive, negative, or zero. In particular, as Fig. 3(a) also shows, there is a critical value of the droplet radius, denoted by $b_{\mathrm{c}} = b_{\mathrm{c}}(m)$ ($0 \leqslant b_{\mathrm{c}} \leqslant 1$), which depends on m according to the equation

$$f_{\mathrm{M}}(b_{\mathrm{c}},m) = 0, \tag{47}$$

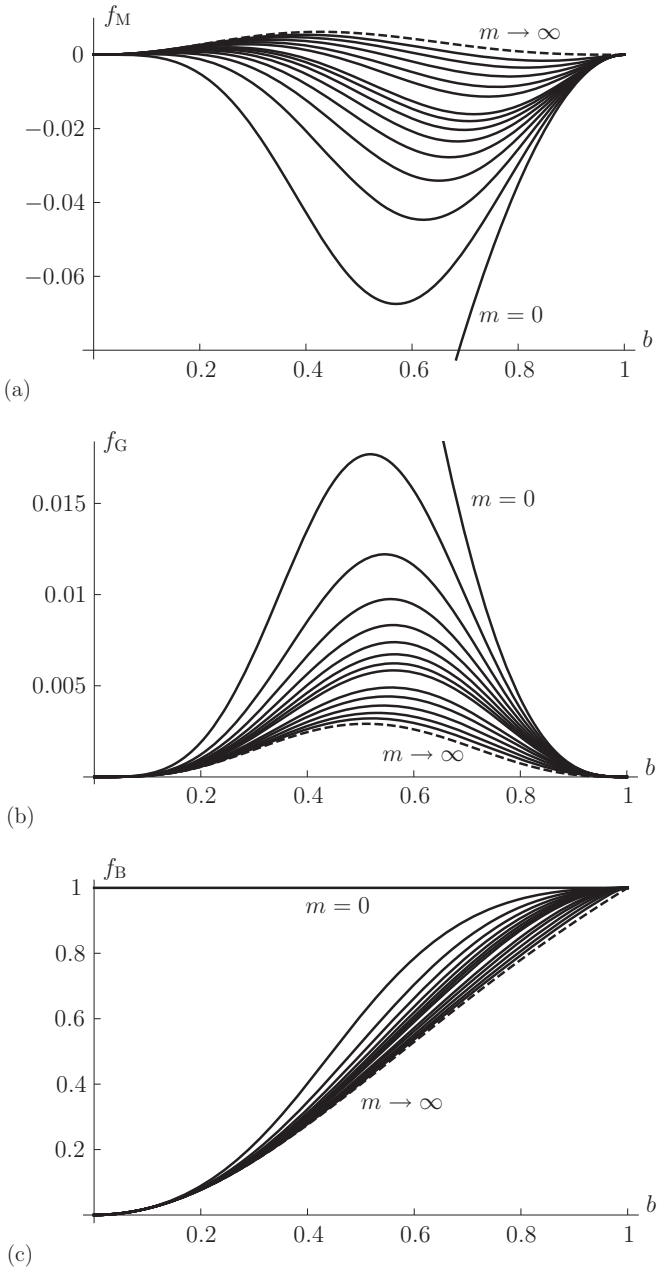

FIG. 3. Plots of the functions f_j for $j = \mathrm{M}, \mathrm{G}, \mathrm{B}$ defined by Eqs. (38)–(40) which arise in the Marangoni (M), gravitational (G), and background-flow (B) contributions to the fluxes appearing in Eqs. (37) as functions of the droplet radius b for $m = 0, 1/8, 1/4, \ldots, 1, 3/2, 2, 5, 10$ and in the limit $m \to \infty$ given by Eqs. (44)–(46) (the latter shown with dashed lines).

such that f_{M} is positive for $0 < b < b_{\mathrm{c}}$ and negative for $b_{\mathrm{c}} < b < 1$. As we shall see, the critical droplet radius b_{c} plays an important role in the motion of the droplet, and so Fig. 4 shows b_{c} calculated from Eq. (47) plotted as a function of m. In particular, Fig. 4 shows that b_{c} is

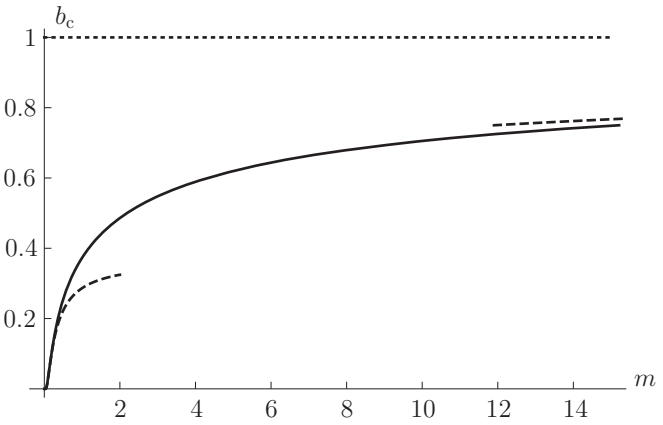

FIG. 4. Plot of the critical droplet radius b_c calculated from Eq. (47) as a function of the viscosity ratio m. The asymptotic expressions $b_c \sim \exp[-1/(4m) - 1] \to 0$ in the limit $m \to 0^+$ and $b_c \sim 1 - (3/2m)^{1/2} + (5/4m) \to 1^-$ in the limit $m \to \infty$ are shown with dashed lines.

a monotonically increasing function of m satisfying $b_c \sim \exp[-1/(4m) - 1] \to 0^+$ in the limit $m \to 0^+$ and $b_c \sim 1 - (3/2m)^{1/2} + (5/4m) \to 1^-$ in the limit $m \to \infty$.

Now that the velocities, and hence the fluxes, are known, the evolution of the shape of the droplet is governed by the kinematic condition (31). The evolution of $b(t)$ and $L(t)$ is analyzed in Sec. IV. Once the evolution of the shape of the droplet has been determined, we can determine the evolution of its position within the tube by considering the motion of the ends of the droplet. The evolution of $z_f(t)$, $z_b(t)$, and $c(t)$ is analyzed in Sec. V.

IV. EVOLUTION OF THE SHAPE OF THE DROPLET

Using Eq. (37), the kinematic condition (31) leads to the equation governing the evolution of the radius $b(t)$, and hence of the length $L(t)$, of the droplet, namely,

$$\frac{db}{dt} = -\frac{M f_M(b, m)}{2b}, \tag{48}$$

where f_M is given by Eq. (38). Equation (48) is a separable differential equation, with implicit solution $t = t(b)$ given by

$$t = \frac{2}{M} \int_b^{b_0} \frac{\tilde{b}}{f_M(\tilde{b}, m)}\, d\tilde{b}, \tag{49}$$

where the initial value of b is denoted by $b_0 = b(0)$ (with the corresponding initial value of L denoted by $L_0 = L(0) = 1/b_0^2$). However, since the integral in Eq. (48) cannot, in general, be evaluated in closed form, we investigated b numerically via Eq. (48) and asymptotically via Eq. (49).

An important observation is that, since the gravitational and background-flow contributions to Q_1 and $-Q_2$ given by Eq. (37) are independent of z, they do not appear in Eq. (48), and hence the evolution of b and L is driven *entirely* by Marangoni effects (i.e., is independent of gravitational and background-flow effects). In particular, in the absence of Marangoni effects ($M = 0$), but not, in general, when they are present, b and L are constants (i.e., the droplet moves without changing shape). Moreover, since M can be removed explicitly from Eqs. (48) and (49) by an appropriate rescaling of time, changing the value of M changes the time scale, but not the qualitative behavior, of the evolution of b and L.

Inspection of Eq. (48) with f_M given by Eq. (38) shows that, regardless of the values of $\Delta\rho$ and Q_b, when $0 < b < b_c$ then b always decreases and hence L always increases in time, but when

$b_c < b < 1$ then b always increases and hence L always decreases in time. In particular, this means that when the initial radius b_0 satisfies $0 < b_0 < b_c$ the droplet becomes narrower and longer as time increases, but when it satisfies $b_c < b_0 < 1$ the droplet becomes wider and shorter as time increases, ultimately filling the entire cross section of the tube as $t \to \infty$. Specifically, Eq. (49) shows that

$$b \sim b_0 - \frac{M f_M(b_0, m)}{2b_0} t, \quad L \sim L_0 + M f_M(b_0, m) L_0^2 t \tag{50}$$

as $t \to 0^+$, and that

$$b \sim \frac{4}{Mt\left[\ln\frac{Mt}{4} - \left(1 + \frac{1}{4m}\right)\right]} \to 0, \quad L \sim \frac{M^2 t^2}{16}\left[\ln\frac{Mt}{4} - \left(1 + \frac{1}{4m}\right)\right]^2 \to \infty \tag{51}$$

as $t \to \infty$ when $0 < b_0 < b_c$, whereas

$$b \sim 1 - \frac{2}{Mt} \to 1^-, \quad L \sim 1 + \frac{4}{Mt} \to 1^+ \tag{52}$$

as $t \to \infty$ when $b_c < b_0 < 1$. In particular, in the special case of an inviscid bubble ($m = 0$) then $b_c = 0$ and hence the droplet *always* becomes wider and shorter, whereas in the special case of an inviscid surrounding fluid ($m \to \infty$) then $b_c \to 1^-$ and hence the droplet *always* becomes narrower and longer.

Figure 5 shows the evolution of b and L calculated numerically from Eq. (48) for various b_0 and $L_0 = 1/b_0^2$ in the case $m = 1$ and $M = 1$. In particular, Fig. 5 illustrates how the critical values $b = b_c$ and $L = L_c = 1/b_c^2$ separate droplets that become narrower and longer from those that become wider and shorter.

At first sight, the fact that the droplet may either expand or contract might seem rather surprising as, regardless of the value of m, σ is a quadratic function of z given by Eq. (34), and hence Marangoni effects always drive flow away from $z = 0$, and so we might naively expect the droplet always to become wider and shorter. However, while, as we have seen, this is true for an inviscid bubble with $m = 0$, it is not, in general, true for a viscous droplet with $m \neq 0$, in which case the change in the shape of the droplet depends on the relative strengths of the Marangoni-induced flows in the two fluids. Specifically, for a droplet satisfying $0 < b < b_c$ the flux of the Marangoni-driven axial flow in the droplet is a linearly increasing function of z, whereas that of the surrounding fluid is a linearly decreasing function of z, with the result that the droplet expands axially and contracts radially. On the other hand, for a droplet satisfying $b_c < b < 1$ the opposite occurs, with the result that the droplet contracts axially and expands radially.

Note that the behavior described in this section is qualitatively different from that for ordinary fluids for which σ is a linearly decreasing function of T analyzed by Wilson [25]. In the latter case the Marangoni contribution to Q_1 and $-Q_2$ is independent of z, and hence b and L are constants (i.e., the droplet always moves without changing shape).

V. EVOLUTION OF THE POSITION OF THE DROPLET

As we showed in the previous section, the present model predicts that the evolution of the shape of the droplet is driven entirely by Marangoni effects (i.e., it is independent of gravitational and background-flow effects). However, as we now describe, the evolution of the position of the droplet depends, in general, on all three effects.

In order to determine the evolution of the position of the droplet we need to determine the evolution of the positions of the front, $z = z_f(t)$, and the back, $z = z_b(t)$, and hence of the center of mass, $z = c(t) = (z_f(t) + z_b(t))/2$, of the droplet. In general, the details of the flow near the ends of the droplet will be complicated, but, since we are interested in the overall motion of the droplet rather than the details of the flow near its ends, a simple but realistic modeling assumption is that the motion of each end is due to the flux of fluid 1 at that end, i.e., we take the motion of the front

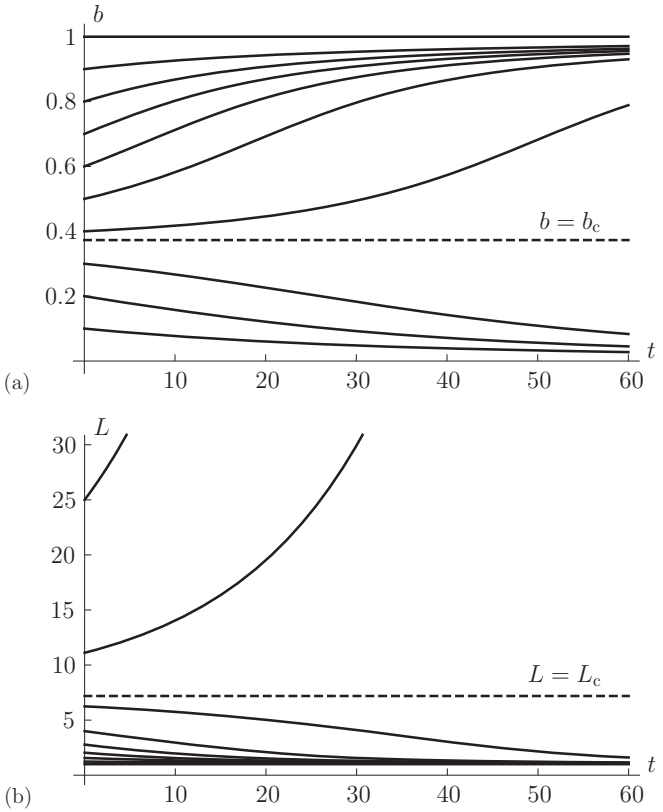

FIG. 5. Evolution of (a) the radius b and (b) the length L of the droplet calculated numerically from Eq. (48) for various initial radii b_0 and initial lengths $L_0 = 1/b_0^2$ in the case $m = 1$ and $M = 1$. The critical values $b = b_c \simeq 0.3729$ and $L = L_c = 1/b_c^2 \simeq 7.1899$ are shown with dashed lines.

and of the back of the droplet to be governed by

$$b^2 \frac{dz_f}{dt} = Q_1|_{z=z_f(t)} \quad \text{and} \quad b^2 \frac{dz_b}{dt} = Q_1|_{z=z_b(t)}, \tag{53}$$

respectively. Adding together the two equations in (53) [41] yields

$$b^2 \frac{dc}{dt} = \frac{1}{2}[Q_1|_{z=z_f(t)} + Q_1|_{z=z_b(t)}], \tag{54}$$

which, since Q_1 given by Eq. (37) is a linear function of z, reduces to

$$b^2 \frac{dc}{dt} = Q_1|_{z=c(t)}, \tag{55}$$

leading to the equation governing the evolution of the center of mass of the droplet, $c(t)$, namely,

$$\frac{dc}{dt} = \frac{Mcf_M(b,m) + \Delta\rho f_G(b,m) + Q_b f_B(b,m)}{b^2}, \tag{56}$$

where f_M, f_G, and f_B are given by Eqs. (38), (39), and (40), respectively. With Eq. (48), Eq. (56) has a parametric solution for c (with parameter b) given by

$$c = \frac{b_0^2 c_0}{b^2} - \frac{2}{b^2}\int_{b_0}^{b} \frac{\tilde{b}[\Delta\rho f_G(\tilde{b},m) + Q_b f_B(\tilde{b},m)]}{M f_M(\tilde{b},m)}\, d\tilde{b}, \tag{57}$$

where the initial value of c is denoted by $c_0 = c(0)$. However, as for Eq. (49), since the integral in Eq. (57) cannot, in general, be evaluated in closed form, we investigated c numerically via Eq. (56) and asymptotically via Eq. (57). Once c is known, the positions of the ends of the bubble are given simply by $z_f = c + (L/2)$ and $z_f = c - (L/2)$, respectively.

Equation (56) shows that, unlike the evolution of b and L described in Sec. IV, the evolution of c depends on $\Delta\rho$ and Q_b as well as on M. In particular, Eq. (56) shows that, except in the case in which Marangoni effects are absent ($M = 0$) analyzed in Sec. VI, in which case b and L and hence dc/dt are constants, the velocity of the droplet, dc/dt, is not, in general, constant. Specifically, Eq. (57) shows that

$$c \sim c_0 + \frac{Mc_0 f_M(b_0, m) + \Delta\rho f_G(b_0, m) + Q_b f_B(b_0, m)}{b_0^2} t \tag{58}$$

as $t \to 0^+$, and that the behavior as $t \to \infty$ depends on whether Q_b is zero or nonzero.

In the special case of a closed tube with no background flow, $Q_b = 0$, it is found from Eq. (57) that when $0 < b_0 < b_c$ then $c = O(t \ln t)^2 \to \infty$ as $t \to \infty$ (i.e. that the droplet ultimately moves far away from $z = 0$), but when $b_c < b_0 < 1$ then c approaches a constant value c_∞ according to $c \sim c_\infty[1 + 4/(Mt)] \to c_\infty$ as $t \to \infty$ (i.e., that the droplet ultimately approaches a final stationary position).

In the general case $Q_b \neq 0$ it is found from Eq. (57) that $|c| \to \infty$ as $t \to \infty$ (i.e., that the droplet again ultimately moves far away from $z = 0$). In particular, when $b_c < b_0 < 1$ then $c/Q_b \sim t + O(\ln t)$ as $t \to \infty$, showing that in this case the droplet ultimately moves at a constant velocity determined by the background flow. However, when $0 < b_0 < b_c$ then the behavior of c has a more complicated dependence on t, and so in this case the droplet does not, in general, ultimately move with constant velocity.

In the next four sections we use Eqs. (56) and (57) to determine the evolution of c in four different cases. Specifically, in Sec. VI we consider the case in which Marangoni effects are absent ($M = 0$), in Sec. VII we consider the case in which only Marangoni effects are present ($\Delta\rho = 0$ and $Q_b = 0$), while in Secs. VIII and IX we consider the cases in which either only Marangoni effects and gravitational effects are present ($Q_b = 0$) or only Marangoni effects and background-flow effects are present ($\Delta\rho = 0$), respectively. In each case, since the evolution of b and L has already been determined in Sec. IV, we need only determine the evolution of c to complete the description of the motion of the droplet.

Note that, once again, the behavior described in this section is qualitatively different from that for ordinary fluids for which σ is a linearly decreasing function of T studied by Wilson [25]. In the latter case b and L are constants and the Marangoni contribution to dc/dt is independent of c, and hence dc/dt is constant (i.e., the velocity of the droplet is always constant).

VI. MARANGONI EFFECTS ARE ABSENT ($M = 0$)

In the case in which Marangoni effects are absent ($M = 0$), $b = b_0$ and $L = L_0$ are constants, and from Eq. (56) the droplet moves with constant velocity

$$\frac{dc}{dt} = \frac{\Delta\rho f_G(b_0, m) + Q_b f_B(b_0, m)}{b_0^2} \tag{59}$$

without changing shape. In particular,

$$\frac{dc}{dt} = \Delta\rho \left[\frac{(1 - b_0^2)(1 - 3b_0^2)}{8b_0^2} - \frac{b_0^2}{2} \ln b_0 \right] + \frac{Q_b}{b_0^2} \tag{60}$$

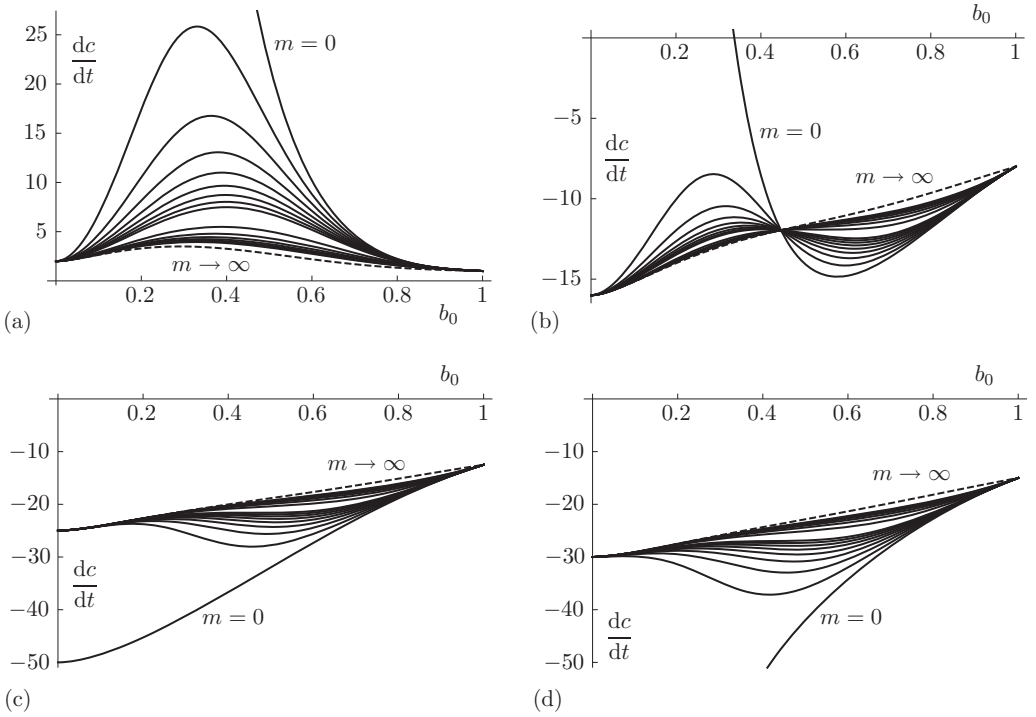

FIG. 6. Plots of the constant velocity of the droplet dc/dt when Marangoni effects are absent given by Eq. (59) as a function of its initial radius b_0 in the case $M = 0$ and $\Delta\rho = 100$ when (a) $Q_b = 1$, (b) $Q_b = -8$, (c) $Q_b = -25/2$, and (d) $Q_b = -15$ for $m = 0, 1/32, 1/16, \ldots, 1/4, 1/2, \ldots, 2$ and in the limit $m \to \infty$ given by Eq. (61) (the latter shown with dashed lines).

when $m = 0$, and

$$\frac{dc}{dt} = -\frac{\Delta\rho b_0^2}{2}\left(\frac{1-b_0^2}{1+b_0^2} + \ln b_0\right) + \frac{2Q_b}{1+b_0^2} \tag{61}$$

in the limit $m \to \infty$.

In this case we may, without loss of generality, take $\Delta\rho > 0$, but Q_b may be positive, negative, or zero. When $Q_b \geqslant 0$ then background-flow and gravitational effects cooperate, and so $dc/dt > 0$ (i.e., the droplet always moves upwards); however, when $Q_b < 0$ then the effects compete, and so dc/dt may be positive, negative, or zero (i.e., the droplet may move upwards, downwards, or remain stationary).

Figure 6 shows dc/dt plotted as a function of b_0 for the full range of values of m for four different values of Q_b satisfying $Q_b > 0$, $-\Delta\rho/8 < Q_b < 0$, $Q_b = -\Delta\rho/8$, and $Q_b < -\Delta\rho/8$, respectively. In particular, Fig. 6 illustrates that, except in the special case of an inviscid bubble $m = 0$ [42], dc/dt is a nonmonotonic function of b_0, with either a maximum and a minimum (when $Q_b < 0$) or just a maximum (when $Q_b \geqslant 0$) between its values $2Q_b$ and Q_b at $b_0 = 0$ and $b_0 = 1$, respectively. Intriguingly, Fig. 6(b) also illustrates that when $-\Delta\rho/8 < Q_b < 0$, droplets with radius $b_0 = [1 - (-8Q_b/\Delta\rho)^{1/2}]^{1/2}$ have the same velocity, namely, $dc/dt = -\Delta\rho(1 - b_0^2 + 2b_0^2 \ln b_0)/4$, for *all* values of m.

VII. ONLY MARANGONI EFFECTS ARE PRESENT ($\Delta\rho = 0$ and $Q_b = 0$)

In the case in which only Marangoni effects are present ($\Delta\rho = 0$ and $Q_b = 0$), then b and L evolve as described in Sec. IV, and from Eq. (57) the position of the center of mass of the droplet is

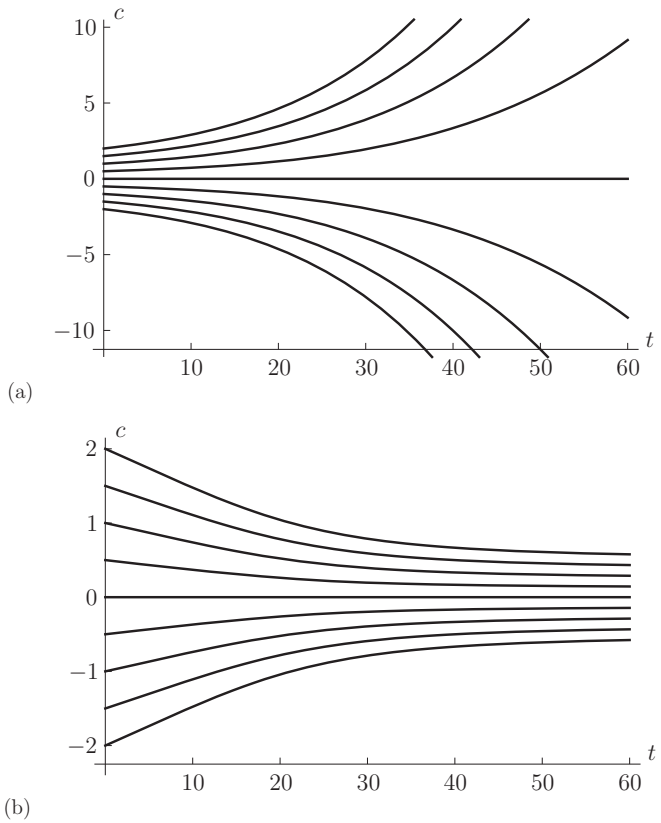

FIG. 7. Evolution of the position of the center of mass of the droplet c when only Marangoni effects are present given by Eq. (62) for initial positions $c_0 = -2, -3/2, -1, \ldots, 2$ in the case $m = 1$, $M = 1$, $\Delta\rho = 0$, and $Q_b = 0$ when (a) $b_0 = 1/4$ ($< b_c \simeq 0.3729$) and (b) $b_0 = 1/2$ ($> b_c$).

given by

$$c = \frac{b_0^2 c_0}{b^2} = b_0^2 c_0 L, \tag{62}$$

and hence the positions of the ends of the droplet are given by $z_f = (b_0^2 c_0 + (1/2))L$ and $z_b = (b_0^2 c_0 - (1/2))L$.

Figure 7 shows the evolution of c for various c_0 for two different values of b_0, one satisfying $0 < b_0 < b_c$ and the other satisfying $b_c < b_0 < 1$. In particular, Fig. 7(a) illustrates that when $0 < b_0 < b_c$ then c/c_0 is an increasing function of t satisfying $c/c_0 \to \infty$ as $t \to \infty$ (i.e., the droplet always moves away from $z = 0$), whereas when $b_c < b_0 < 1$ then c/c_0 is a decreasing function of t satisfying $c/c_0 \to c_\infty/c_0 = b_0^2$ (<1) as $t \to \infty$ (i.e., the droplet always moves towards $z = 0$). Note that both parts of Fig. 7 are symmetric about $c = 0$, reflecting the symmetry of σ given by Eq. (34) about $z = 0$.

Combining these results for the evolution of c with those for the evolution of b and L described in Sec. IV, Fig. 8 shows examples of the four qualitatively different forms of the evolution of a droplet when only Marangoni effects are present when $c_0 > 0$, illustrating that when $0 < b_0 < b_c$ the droplet becomes narrower and longer and moves away from $z = 0$ (in particular, satisfying $b \to 0^+$, $L \to \infty$, and $c/c_0 \to \infty$ as $t \to \infty$) as shown in Figs. 8(a) and 8(b), whereas when $b_c < b_0 < 1$ the droplet becomes wider and shorter and moves towards $z = 0$, ultimately filling the entire

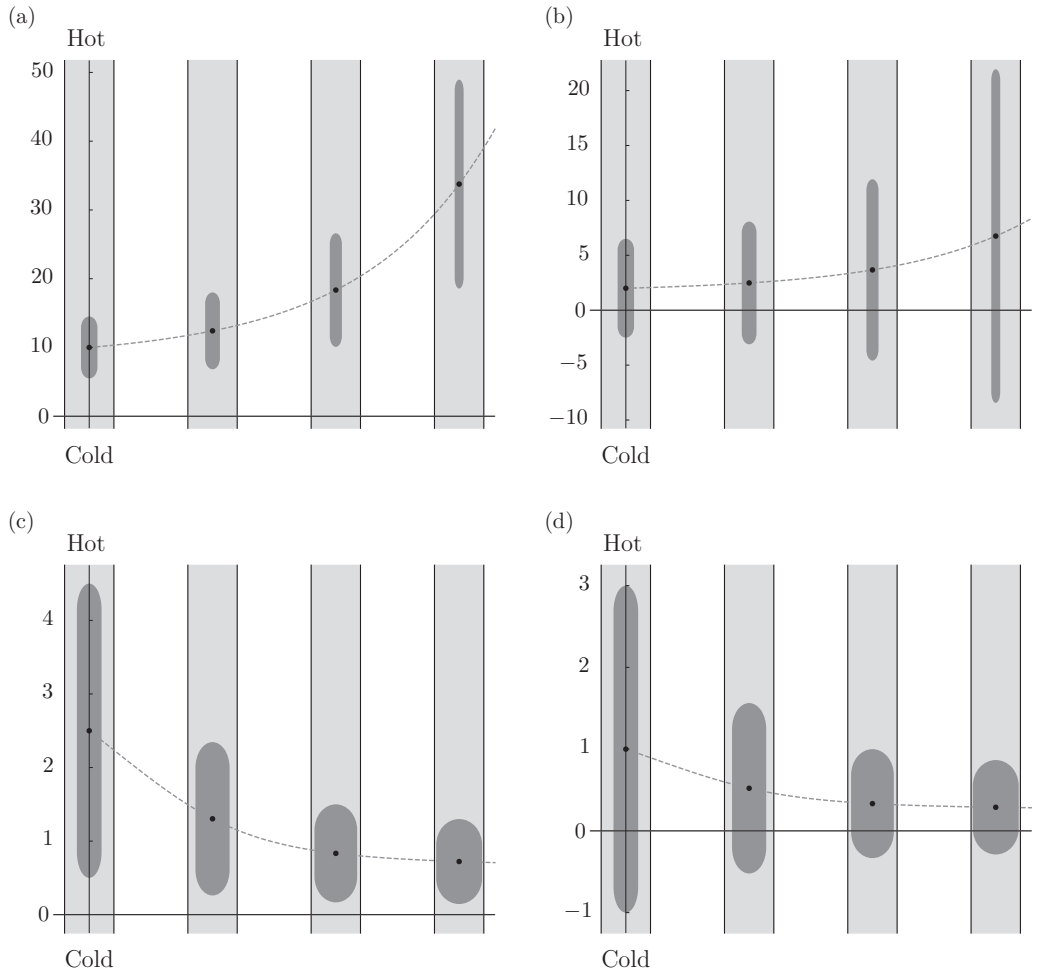

FIG. 8. Examples of the four qualitatively different forms of the evolution of a droplet when only Marangoni effects are present when $c_0 > 0$ in the case $m = 1$, $M = 1$, $\Delta\rho = 0$, $Q_b = 0$, for which $b_c \simeq 0.3729$. In (a) and (b), $L_0 = 9$, $b_0 = 1/3$ ($<b_c$), with (a) $c_0 = 10$, (b) $c_0 = 2$, and the snapshots are shown at $t = 0$, 15, 30, 45, whereas in (c) and (d), $L_0 = 4$, $b_0 = 1/2$ ($>b_c$), with (c) $c_0 = 5/2$, (d) $c_0 = 1$, and the snapshots are shown at $t = 0$, 20, 40, 60. In each snapshot the center of mass of the droplet is denoted by a dot (•). Note that the corresponding evolutions when $c_0 < 0$ are simply the mirror images of those when $c_0 > 0$ in the plane $z = 0$, and the evolutions when $c_0 = 0$ have $c \equiv 0$ for all t.

cross section of the tube at a final stationary position which is closer to $z = 0$ than its original position (in particular, satisfying $b \to 1^-$, $L \to 1^+$, and $c/c_0 \to c_\infty/c_0 = b_0^2$ (<1) as $t \to \infty$) as shown in Figs. 8(c) and 8(d). Note that in Figs. 8(a) and 8(c) the entire droplet is initially (and always remains) above $z = 0$, whereas in Figs. 8(b) and 8(d) the back of the droplet is initially (and always remains) below $z = 0$. Because of the symmetry of σ given by Eq. (34) about $z = 0$, the corresponding evolutions when $c_0 < 0$ are simply the mirror images of those when $c_0 > 0$ in the plane $z = 0$, and the evolutions when $c_0 = 0$ have $c \equiv 0$ for all t (i.e., the droplet changes shape symmetrically with its center of mass remaining stationary at $z = 0$).

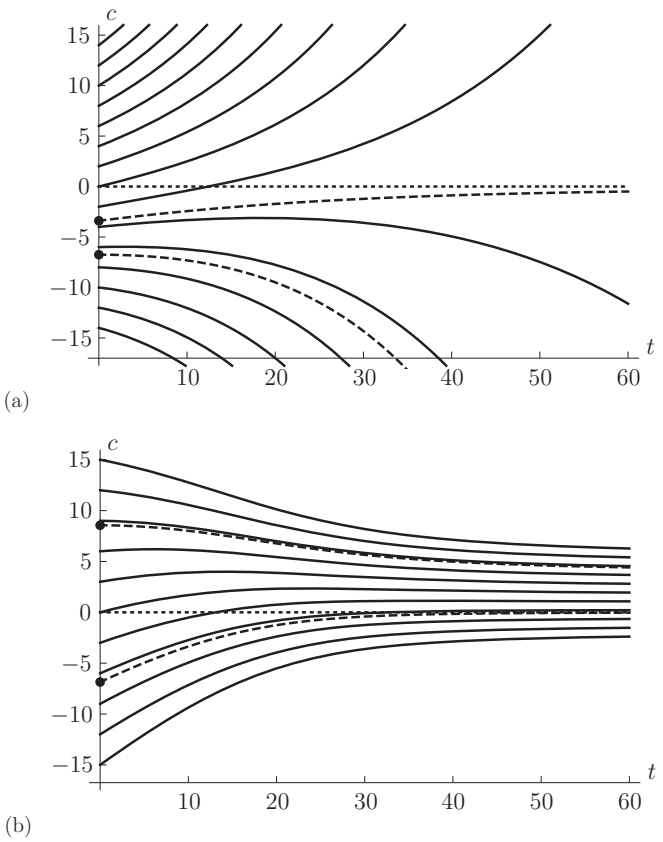

FIG. 9. Evolution of the position of the center of mass of the droplet c when only Marangoni and gravitational effects are present given by Eq. (57) in the case $m = 1$, $M = 1$, $\Delta\rho = 10$, and $Q_b = 0$ for initial positions (a) $c_0 = -14, -12, -10, \ldots, 12, 14$ when $b_0 = 1/4\,(< b_c \simeq 0.3729)$ and (b) $c_0 = -15, -12, -9, \ldots, 12, 15$ when $b_0 = 1/2\,(> b_c)$. The evolutions corresponding to the critical values (a) $c_0 = c_1^G \simeq -6.7523$ and $c_0 = c_2^G \simeq -3.3930$, and (b) $c_0 = c_1^G \simeq 8.5571$ and $c_0 = c_2^G \simeq -6.8558$, which separate the three different behaviors, are shown with dashed lines.

VIII. ONLY MARANGONI AND GRAVITATIONAL EFFECTS ARE PRESENT ($Q_b = 0$)

In the case in which only Marangoni and gravitational effects are present ($Q_b = 0$), then b and L evolve as described in Sec. IV, and the position of the center of mass of the droplet is given by Eq. (57).

In this case we may, without loss of generality, take $\Delta\rho > 0$, and, like the case in which only Marangoni effects are present described in Sec. VII, despite the fact that M is non-negative, the droplet may move upwards or downwards. However, in contrast to the case described in Sec. VII, in this case the droplet cannot remain stationary, and the competition between Marangoni and gravitational effects can lead to a nonmonotonic evolution of c. In particular, recall from Sec. V that since $Q_b = 0$ then when $0 < b_0 < b_c$ then $c = O(t \ln t)^2 \to \infty$ as $t \to \infty$ (i.e., that the droplet ultimately moves far away from $z = 0$), but when $b_c < b_0 < 1$ then c approaches a constant value c_∞ according to $c \sim c_\infty[1 + 4/(Mt)] \to c_\infty$ as $t \to \infty$ (i.e., that the droplet ultimately approaches a final stationary position).

Figure 9 shows the evolution of c for various c_0 for two different values of b_0, one satisfying $0 < b_0 < b_c$ and the other satisfying $b_c < b_0 < 1$.

First, consider the case of a droplet satisfying $0 < b_0 < b_c$ shown in Fig. 9(a), for which, as we have already described in Sec. IV, $b \to 0^+$ and $L \to \infty$ as $t \to \infty$. In this case Eq. (57) shows that $|c| \to \infty$ according to

$$c \sim \frac{k}{b^2} \tag{63}$$

as $t \to \infty$, where

$$k = b_0^2 c_0 + \frac{2\Delta\rho}{M} \int_0^{b_0} \frac{b f_G(b,m)}{f_M(b,m)}\, db \tag{64}$$

is a constant. In particular, Fig. 9(a) shows that there are three qualitatively different possible evolutions of c depending on the value of c_0 in relation to two critical values, denoted by c_1^G and c_2^G, where $c_1^G < c_2^G$. Specifically, when $c_0 > c_2^G$ then c increases monotonically, when $c_1^G < c_0 < c_2^G$ then c first increases to a maximum and then decreases, and when $c_0 < c_1^G$ then c decreases monotonically, where the critical value c_1^G is the value of c_0 for which $dc/dt(0) = 0$, which from Eq. (58) is given by

$$c_1^G = -\frac{\Delta\rho f_G(b_0,m)}{M f_M(b_0,m)}, \tag{65}$$

and the critical value c_2^G is the value of c_0 for which $k = 0$, namely,

$$c_2^G = -\frac{2\Delta\rho}{M b_0^2} \int_0^{b_0} \frac{b f_G(b,m)}{f_M(b,m)}\, db. \tag{66}$$

Second, consider the case of a droplet satisfying $b_c < b_0 < 1$ shown in Fig. 9(b), for which, as we already described in Sec. IV, $b \to 1^-$ and $L \to 1^+$ as $t \to \infty$. In this case Eq. (57) shows that $c \to c_\infty$ as $t \to \infty$, where

$$c_\infty = b_0^2 c_0 - \frac{2\Delta\rho}{M} \int_{b_0}^1 \frac{b f_G(b,m)}{f_M(b,m)}\, db. \tag{67}$$

Specifically, Fig. 9(b) shows that there are again three qualitatively different possible evolutions of c depending on the value of c_0 in relation to two critical values, again denoted by c_1^G and c_2^G, where now $c_1^G > c_2^G$. Specifically, when $c_0 > c_1^G$ then c decreases monotonically, when $c_2^G < c_0 < c_1^G$ then c first increases to a maximum and then decreases, and when $c_0 < c_2^G$ then c increases monotonically, where the critical value c_1^G is again given by Eq. (65) but the critical value c_2^G is now the value of c_0 for which $c_\infty = 0$, namely,

$$c_2^G = \frac{2\Delta\rho}{M b_0^2} \int_{b_0}^1 \frac{b f_G(b,m)}{f_M(b,m)}\, db. \tag{68}$$

IX. ONLY MARANGONI AND BACKGROUND-FLOW EFFECTS ARE PRESENT ($\Delta\rho = 0$)

In the case in which only Marangoni and background-flow effects are present ($\Delta\rho = 0$), then b and L evolve as described in Sec. IV, and the position of the center of mass of the droplet is given by Eq. (57).

In this case we may, without loss of generality, take $Q_b > 0$, and, like the case in which Marangoni and gravitational effects are present as described in Sec. VIII, despite the fact that M is non-negative, the droplet may again move upwards or downwards. Moreover, like in the case described in Sec. VIII, in this case the droplet cannot remain stationary, and the competition between Marangoni and background-flow effects can lead to a similar (but not exactly equivalent) nonmonotonic evolution of c. In particular, recall from Sec. V that since $Q_b \neq 0$ then $|c| \to \infty$ as $t \to \infty$ (i.e., that the droplet ultimately moves far away from $z = 0$).

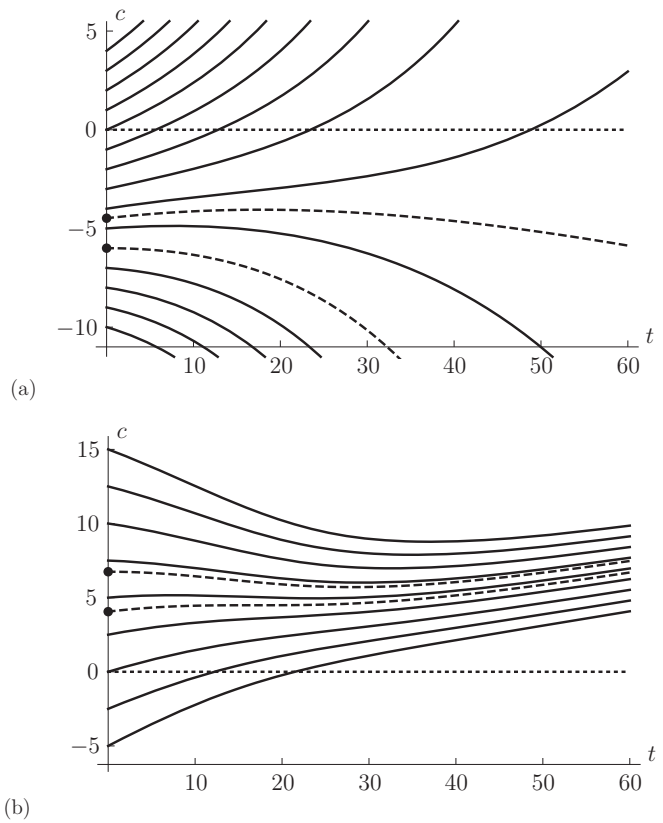

FIG. 10. Evolution of the position of the center of mass of the droplet c when only Marangoni and background-flow effects are present given by Eq. (57) in the case $m = 1$, $M = 1$, $\Delta\rho = 0$, and $Q_b = 1/10$ for initial positions (a) $c_0 = -10, -9, -8, \ldots, 3, 4$ when $b_0 = 1/4\,(< b_c \simeq 0.3729)$ and (b) $c_0 = -5, -5/2, 0, \ldots, 25/2, 15$ when $b_0 = 1/2\,(> b_c)$. The evolutions corresponding to the critical values (a) $c_0 = c_1^B \simeq -5.9993$ and $c_0 = c_2^B \simeq -4.4817$, and (b) $c_0 = c_1^B \simeq 6.7484$ and $c_0 = c_2^B \simeq 4.0561$, which separate the three different behaviors, are shown with dashed lines.

Figure 10 shows typical evolutions of c for various c_0 for two different values of b_0, one satisfying $0 < b_0 < b_c$ and the other satisfying $b_c < b_0 < 1$.

First, consider the case of a droplet satisfying $0 < b_0 < b_c$ shown in Fig. 10(a). The evolution of c in this case parallels that shown in Fig. 9(a) (with $\Delta\rho$, f_G, c_1^G, and c_2^G replaced with Q_b, f_B, c_1^B, and c_2^B, respectively), and so the discussion need not be repeated here. The critical values c_1^B and c_2^B, where $c_1^B < c_2^B$, are given by

$$c_1^B = -\frac{Q_b f_B(b_0, m)}{M f_M(b_0, m)} \tag{69}$$

and

$$c_2^B = -\frac{2Q_b}{Mb_0^2}\int_0^{b_0} \frac{b f_B(b, m)}{f_M(b, m)}\, db. \tag{70}$$

Second, consider the case of a droplet satisfying $b_c < b_0 < 1$ shown in Fig. 10(b). In this case Eq. (57) shows that $c \sim Q_b t \to \infty$ as $t \to \infty$, and the evolution of c in this case is similar to, but qualitatively different from, that shown in Fig. 9(b). Specifically, when $c_0 > c_1^B$ then c first decreases and then increases with t, when $c_2^B < c_0 < c_1^B$ then c first increases, then decreases, and

then increases again, and when $c_0 < c_2^{\mathrm{B}}$ then c increases monotonically with t. The critical value c_1^{B} is defined in the same way that c_1^{G} was in Sec. VIII, and so is again given by Eq. (69). However, since there is now no value of c_0 that leads to a constant value of c as $t \to \infty$, the critical value c_2^{B} is not defined in the way that c_2^{G} was in Sec. VIII. Instead, c_2^{B} is determined as the value of c_0 for which the maximum, the minimum, and the point of inflection of the solution c coincide, so that $dc/dt = 0$ and $d^2c/dt^2 = 0$. With Eq. (48) these lead to the condition

$$f_{\mathrm{B}} \frac{\partial f_{\mathrm{M}}}{\partial b} - f_{\mathrm{M}} \frac{\partial f_{\mathrm{B}}}{\partial b} = 0 \tag{71}$$

determining the value $b = b_{\mathrm{SP}}$ of b corresponding to the stationary value $c = c_{\mathrm{SP}}$ of c. Equation (56) then gives $c_{\mathrm{SP}} = -Q_{\mathrm{b}} f_{\mathrm{B}}/M f_{\mathrm{M}}$ evaluated at $b = b_{\mathrm{SP}}$, and so c_2^{B} is obtained from Eq. (57) as

$$c_2^{\mathrm{B}} = \frac{Q_{\mathrm{b}}}{M b_0^2} \left(2 \int_{b_0}^{b} \frac{\tilde{b} f_{\mathrm{B}}}{f_{\mathrm{M}}} \, d\tilde{b} - \frac{b^2 f_{\mathrm{B}}}{f_{\mathrm{M}}} \right) \Bigg|_{b=b_{\mathrm{SP}}}. \tag{72}$$

X. CONCLUSIONS

In the present work we formulated and analyzed a theoretical model for the unsteady motion of a long bubble or droplet in a self-rewetting system in a nonuniformly heated tube due to a combination of Marangoni effects, gravitational effects due to the density difference between the two fluids, and an imposed background flow along the tube.

We found that the present model predicts that the evolution of the shape of the droplet is driven entirely by Marangoni effects, and depends on the initial value of its radius b_0 in relation to the critical value $b_{\mathrm{c}} = b_{\mathrm{c}}(m)$ given by Eq. (47). Specifically, as described in Sec. IV, when $0 < b_0 < b_{\mathrm{c}}$ the droplet becomes narrower and longer as time increases, but when $b_{\mathrm{c}} < b_0 < 1$ the droplet becomes wider and shorter as time increases, ultimately filling the entire cross section of the tube as $t \to \infty$. However, as described in Sec. V, the evolution of the position of the droplet depends, in general, on gravitational and background-flow effects in addition to Marangoni effects. In the case in which Marangoni effects are absent the droplet always moves with constant velocity given by Eq. (59) without changing shape. In the case in which only Marangoni effects are present when $0 < b_0 < b_{\mathrm{c}}$ the droplet always moves away from $z = 0$ as time increases, but when $b_{\mathrm{c}} < b_0 < 1$ the droplet moves towards $z = 0$ as time increases, ultimately filling the entire cross section of the tube at a final stationary position which is closer to $z = 0$ than its original position. Figure 8 shows examples of the four qualitatively different forms of the evolution of the droplet in this case. In the cases in which either only Marangoni effects and gravitational effects or only Marangoni effects and background-flow effects are present the competition between the two effects can lead to a nonmonotonic evolution of c.

For completeness, the corresponding results for the closely related problem of a two-dimensional droplet in a channel are presented in Appendix B.

Finally, it should be reiterated that the behavior of a self-rewetting system described in the present work is qualitatively different from that for ordinary fluids, in which case the droplet always moves with constant velocity without changing shape.

ACKNOWLEDGMENTS

All four authors gratefully acknowledge the financial support provided by The Carnegie Trust for the Universities of Scotland via Research Incentive Grant (RIG) No. 70775, "Mathematical Modelling and Analysis of Self-Rewetting Fluids in Heat Pipes." K.S. also acknowledges the financial support of the Engineering and Physical Sciences Research Council (EPSRC) via Research Grant No. EP/N011341/1, "Flow Boiling and Condensation of Mixtures in Microscale."

APPENDIX A: EXPRESSIONS FOR THE PRESSURE GRADIENTS AND THE VELOCITIES OF BOTH FLUIDS

In this Appendix we obtain the expressions for the pressure gradients and velocities of both fluids.

With the pressures of both fluids, p_i for $i = 1, 2$, satisfying Eq. (35), integration of Eqs. (9) twice with respect to r introduces four unknown functions of z and t, which, along with the two unknown pressure gradients, $\partial p_i/\partial z$, means that there are a total of six unknown functions to determine. These functions are determined from Eq. (16) on $r = 0$, Eq. (19) on $r = 1$, Eqs. (22) and (26) with T_i for $i = 1, 2$ given by Eq. (33) on $r = b$, and Eq. (30) with Q_i for $i = 1, 2$ given by Eq. (6), together with $\partial p_1/\partial z - \partial p_2/\partial z = Mz/b$ (obtained by differentiation of Eq. (36) with respect to z), leading to the expressions for the axial components of velocity w_i and the pressure gradients $\partial p_i/\partial z$. Then integration of Eqs. (7) subject to Eq. (15) on $r = 0$ and Eq. (18) on $r = 1$ leads to expressions for the radial components of velocity u_i (which automatically satisfy Eq. (21) on $r = b$). Specifically, the pressure gradients are given by

$$\frac{\partial p_1}{\partial z} = \frac{Mmz(1-b^2)(1+3b^2) - \Delta\rho mb(1-b^2)^2 - 8Q_{\rm b}mb}{b[m-(m-1)b^4]} - \rho_1, \quad \frac{\partial p_2}{\partial z} = \frac{\partial p_1}{\partial z} - \frac{Mz}{b}, \tag{A1}$$

and the velocity components are given by

$$u_1 = \frac{Mr}{16b}\left[-\frac{(1-b^2)[4(m-1)b^4 + b^2(3r^2-4m-2)+r^2]}{m-(m-1)b^4} + 4b^2\ln b\right], \tag{A2}$$

$$\begin{aligned} w_1 = {} & \frac{Mz}{4b}\left[\frac{(1-b^2)[2(m-1)b^4 + b^2(3r^2-2m-1)+r^2]}{m-(m-1)b^4} - 2b^2\ln b\right] \\ & + \frac{\Delta\rho}{4}\left[\frac{(1-b^2)[2(m-1)b^4 + b^2(r^2-2m+1)-r^2]}{m-(m-1)b^4} - 2b^2\ln b\right] \\ & + \frac{2Q_{\rm b}[(1-m)b^2+m-r^2]}{m-(m-1)b^4}, \end{aligned} \tag{A3}$$

$$u_2 = \frac{Mb}{16r}\left[-\frac{(1-r^2)[2(m-1)b^4 - (2m+1)b^2(1-r^2) - 2mr^2]}{m-(m-1)b^4} + 4r^2\ln r\right], \tag{A4}$$

$$\begin{aligned} w_2 = {} & \frac{Mbz}{4}\left[\frac{(1-r^2)[(2m+1)b^2-2m]}{m-(m-1)b^4} - 2\ln r\right] \\ & + \frac{\Delta\rho b^2}{4}\left[\frac{(1-r^2)[(2m-1)b^2-2m]}{m-(m-1)b^4} - 2\ln r\right] + \frac{2Q_{\rm b}m(1-r^2)}{m-(m-1)b^4}. \end{aligned} \tag{A5}$$

Figure 11 shows the radial velocity u_1 and the normalized axial velocity w_1/z at the interface $r = b$ when only Marangoni effects are present plotted as functions of b for the full range of values of m in the case $M = 1$, $Q_{\rm b} = 0$, and $\Delta\rho = 0$. In particular, Fig. 11 shows that u_1 and w_1 are nonmonotonic functions of b satisfying $u_1 < 0$ for $0 < b < b_{\rm c}$, $u_1 > 0$ for $b_{\rm c} < b < 1$, and $w_1 > 0$ for $0 < b < 1$.

APPENDIX B: CORRESPONDING RESULTS FOR A TWO-DIMENSIONAL DROPLET IN A CHANNEL

In this Appendix for completeness we briefly summarize the corresponding results for the closely related problem of a two-dimensional droplet with constant volume (per unit width) $V = 2bL$, semi-width $b = b(t)$, and length $L = L(t)$ in a nonuniformly heated channel of constant semi-width a.

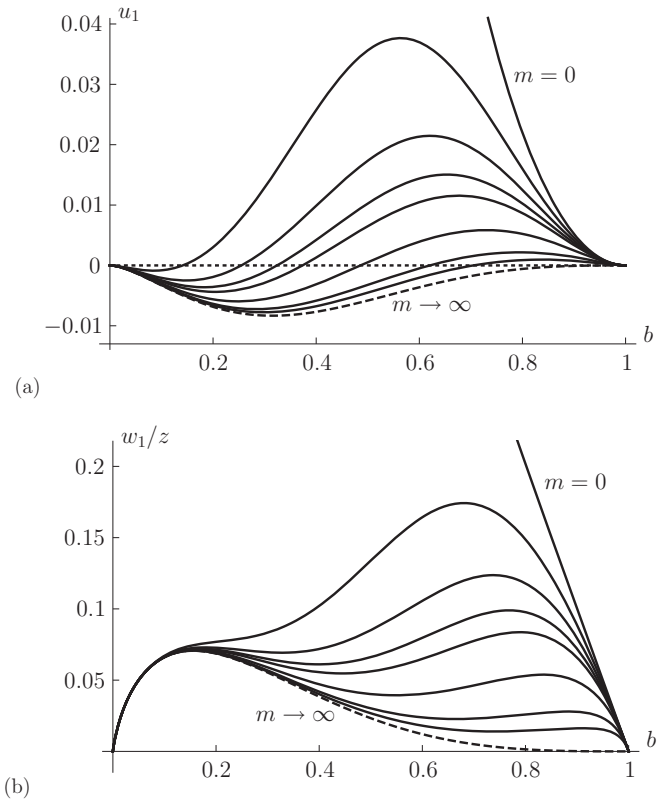

FIG. 11. Plots of (a) the radial velocity u_1 and (b) the normalized axial velocity w_1/z at the interface $r = b$ given by Eqs. (A2) and (A3), respectively, when only Marangoni effects are present as functions of b for $m = 0$, 1/4, 1/2, 3/4, 1, 2, 5, and 10 and in the limit $m \to \infty$ (the latter shown with dashed lines) in the case $M = 1$, $Q_\mathrm{b} = 0$, and $\Delta\rho = 0$.

Referred to Cartesian coordinates $Oxyz$, with the z axis vertically upwards along the centerline of the channel, the walls of the channel are at $x = \pm a$, and, since the problem is symmetric about $x = 0$, we need only consider the flow in $0 \leqslant x \leqslant a$. The geometry of the problem is as sketched in Fig. 2, but with the coordinate r replaced by x. The characteristic axial length scale ℓ and the appropriate nondimensionalization are given by Eqs. (4) and (5), respectively, with r replaced by x and πa^2 replaced by $2a$.

The leading-order governing equations corresponding to Eqs. (7)–(10) are

$$\frac{\partial u_1^*}{\partial x^*} + \frac{\partial w_1^*}{\partial z^*} = 0, \quad \frac{\partial u_2^*}{\partial x^*} + \frac{\partial w_2^*}{\partial z^*} = 0, \tag{B1}$$

$$\frac{\partial p_1^*}{\partial x^*} = 0, \quad \frac{\partial p_2^*}{\partial x^*} = 0, \tag{B2}$$

$$m\frac{\partial^2 w_1^*}{\partial x^{*2}} = \frac{\partial p_1^*}{\partial z^*} + \rho_1^*, \quad \frac{\partial^2 w_2^*}{\partial x^{*2}} = \frac{\partial p_2^*}{\partial z^*} + \rho_2^*, \tag{B3}$$

$$\frac{\partial^2 T_1^*}{\partial x^{*2}} = 0, \quad \frac{\partial^2 T_2^*}{\partial x^{*2}} = 0, \tag{B4}$$

and are subject to the leading-order boundary conditions (15)–(26) with r^* replaced by x^* where appropriate, except for Eq. (25), which is replaced by simply

$$p_1^* - p_2^* = 0. \tag{B5}$$

The semi-width of the droplet, b^*, now satisfies the kinematic condition

$$\frac{db^*}{dt^*} + \frac{\partial Q_1^*}{\partial z^*} = 0, \quad \text{or, equivalently,} \quad \frac{db^*}{dt^*} - \frac{\partial Q_2^*}{\partial z^*} = 0, \tag{B6}$$

while the volume of the droplet is now given by $b^* L^* = 1$, and hence Eq. (32) is replaced by

$$L^* = \frac{1}{b^*}. \tag{B7}$$

Dropping the stars on dimensionless quantities, the temperatures of both fluids are again given by Eq. (33), the pressure gradients are given by

$$\frac{\partial p_1}{\partial z} = \frac{\partial p_2}{\partial z} = \frac{3Mmz(1-b^2) - \Delta\rho m(1-b)^2(2+b) - 3Q_\mathrm{b}m}{2[m-(m-1)b^3]} - \rho_1, \tag{B8}$$

and the velocity components are given by

$$u_1 = \frac{M(1-b)[3b-1-(m-1)(1-b)^3-(1+b)x^2]x}{4[m-(m-1)b^3]}, \tag{B9}$$

$$\begin{aligned} w_1 = {} & \frac{Mz(1-b)[4b^3+m(1-b)^3] + \Delta\rho b(1-b)^2[m(1-b)^2-2b^2] + 3Q_\mathrm{b}m(1-b^2)}{4[m-(m-1)b^3]} \\ & - \frac{[3Mz(1-b^2)+\Delta\rho(1-b)^2(2+b)+3Q_\mathrm{b}](b^2-x^2)}{4[m-(m-1)b^3]}, \end{aligned} \tag{B10}$$

$$u_2 = -\frac{M[m(1-b^2)x - 2b^2(m-(m-1)b)](1-x)^2}{4[m-(m-1)b^3]}, \tag{B11}$$

$$w_2 = (Mz+\Delta\rho b)(1-x) - \frac{[3Mmz(1-b^2)+\Delta\rho b(3m(1-b^2)+2b^2)-3Q_\mathrm{b}m](1-x^2)}{4(m-(m-1)b^3)}. \tag{B12}$$

Figure 12 shows the transverse velocity u_1 and the normalized axial velocity w_1/z at the interface $x = b$ when only Marangoni effects are present plotted as functions of b for the case $M = 1$, $Q_\mathrm{b} = 0$, and $\Delta\rho = 0$. In particular, Fig. 12 shows that u_1 and w_1 are nonmonotonic functions of b satisfying $u_1 < 0$ for $0 < b < b_\mathrm{c}$, $u_1 > 0$ for $b_\mathrm{c} < b < 1$, $w_1 > 0$ for $0 < b < 1$, and $w_1 \to (M/4)^-$ as $b \to 0^+$ (the latter of which is, slightly unexpectedly, qualitatively different from the corresponding behavior in the axisymmetric case shown in Fig. 11).

The axial volume fluxes of fluid 1 and fluid 2, respectively, are given by

$$Q_1 = 2\int_0^b u_1\,dx, \quad Q_2 = 2\int_b^1 u_2\,dx, \tag{B13}$$

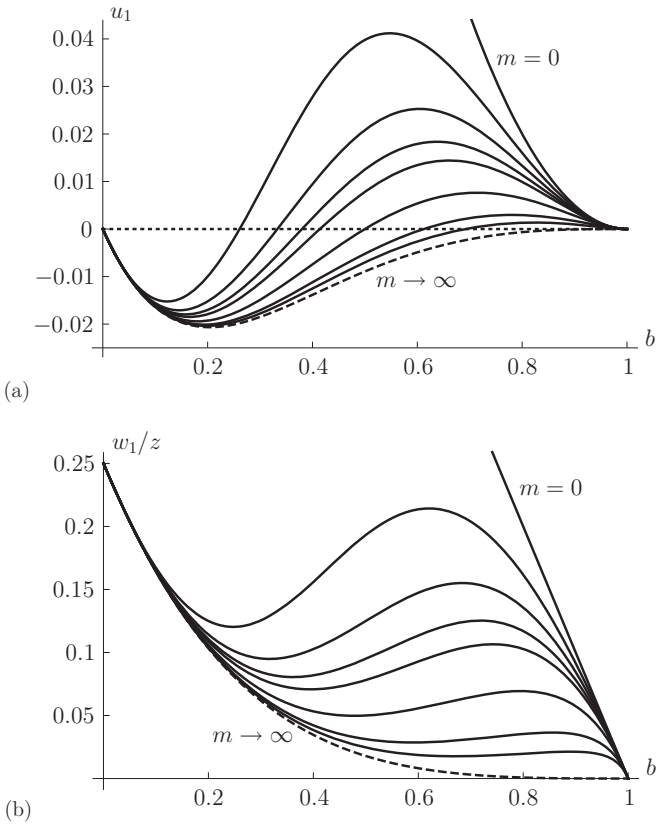

FIG. 12. Plots of (a) the transverse velocity u_1 and (b) the normalized axial velocity w_1/z at the interface $x = b$ given by Eqs. (B9) and (B10), respectively, when only Marangoni effects are present as functions of b for $m = 0$, 1/4, 1/2, 3/4, 1, 2, 5, and 10 and in the limit $m \to \infty$ (the latter shown with dashed lines) in the case $M = 1$, $Q_\mathrm{b} = 0$, and $\Delta\rho = 0$.

which lead again to Eqs. (37), but with the functions f_j for $j = \mathrm{M}, \mathrm{G}, \mathrm{B}$ now defined by

$$f_\mathrm{M}(b, m) = \frac{(1-b)^2 b[m(1-b)^2 - 2b^2]}{2[m - (m-1)b^3]}, \tag{B14}$$

$$f_\mathrm{G}(b, m) = \frac{(1-b)^3 b^2[3m(1-b) + 4b]}{6[m - (m-1)b^3]}, \tag{B15}$$

$$f_\mathrm{B}(b, m) = \frac{b[3m(1-b^2) + 2b^2]}{2[m - (m-1)b^3]}. \tag{B16}$$

These f_j are qualitatively similar to the corresponding functions in the axisymmetric case given by Eqs. (38)–(40) and shown in Fig. 3.

The evolution of the semi-width of the droplet, $b(t)$, is governed by the equation

$$\frac{db}{dt} = -M f_\mathrm{M}(b, m), \tag{B17}$$

which has the implicit solution $t = t(b)$ given by

$$Mt = \phi(b) - \phi(b_0), \tag{B18}$$

where the function $\phi(b)$ is defined by

$$\phi = \frac{1}{1-b} + \frac{3m+2}{2}\ln\left(m - \frac{2b^2}{(1-b)^2}\right) + \frac{7\sqrt{m}}{2\sqrt{2}}\ln\frac{b-b_c}{\hat{b}_c - b} - 2\ln\frac{b}{1-b}, \tag{B19}$$

in which $b_c = b_c(m)$ and $\hat{b}_c = \hat{b}_c(m)$ are the roots of $f_M(b, m) = 0$ given by

$$b_c = \frac{\sqrt{m}}{\sqrt{m}+\sqrt{2}}, \quad \hat{b}_c = \frac{\sqrt{m}}{\sqrt{m}-\sqrt{2}}. \tag{B20}$$

The evolution of b, and hence of L, given by Eq. (B18) is qualitatively similar to that in the axisymmetric case shown in Fig. 5.

The evolution of the position of the center of mass of the droplet, $c(t)$, is governed by

$$\frac{dc}{dt} = \frac{Mcf_M + \Delta\rho f_G + Q_b f_B}{b}, \tag{B21}$$

which has a parametric solution for c (with parameter b) given by

$$c = \frac{b_0 c_0}{b} + \frac{1}{b}(\psi(b) - \psi(b_0)), \tag{B22}$$

where the function $\psi(b)$ is defined by

$$\begin{aligned}\psi = \frac{1}{M}\Bigg\{ & \frac{Q_b}{1-b} + \frac{(1-b)[3m^2(1+b) - 2m(5b-3) - 8(1-b)]\Delta\rho}{6(m-2)^2} - 3mQ_b\ln(1-b) \\ & - \sqrt{2m}\left[Q_b + \frac{(3m^2+6m-8)\Delta\rho}{6(m-2)^3}\right]\ln\frac{\hat{b}_c - b}{b - b_c} \\ & + m\left[\frac{3Q_b}{2} - \frac{(7m-6)\Delta\rho}{3(m-2)^3}\right]\ln[(\hat{b}_c - b)(b - b_c)]\Bigg\}.\end{aligned} \tag{B23}$$

The evolution of $c(t)$, and hence of $z_f(t)$ and $z_b(t)$, given by Eq. (B22) is qualitatively similar to that in the axisymmetric case shown in Figs. 6, 7, 9, and 10.

[1] R. Vochten and G. Petre, Study of the heat of reversible adsorption at the air-solution interface. II. Experimental determination of the heat of reversible adsorption of some alcohols, J. Colloid Interface Sci. **42**, 320 (1973).

[2] G. Petre and M. A. Azouni, Experimental evidence for the minimum of surface tension with temperature at aqueous alcohol solution/air interfaces, J. Colloid Interface Sci. **98**, 261 (1984).

[3] J. C. Legros, Problems related to non-linear variations of surface tension, Acta Astronaut. **13**, 697 (1986).

[4] G. Vázquez, E. Alvarez, and J. M. Navaza, Surface tension of alcohol + water from 20 to 50°C, J. Chem. Eng. Data **40**, 611 (1995).

[5] N. Zhang, Innovative heat pipe systems using a new working fluid, Int. Commun. Heat Mass Transfer **28**, 1025 (2001).

[6] Y. Abe, A. Iwasaki, and K. Tanaka, Microgravity experiments on phase change in self-rewetting fluids, Ann. N.Y. Acad. Sci. **1027**, 269 (2004).

[7] Y. Abe, A. Iwasaki, and K. Tanaka, Thermal management with self-rewetting fluids, Microgravity Sci. Technol. **16**, 148 (2005).

[8] Y. Abe, Self-rewetting fluids, Ann. N.Y. Acad. Sci. **1077**, 650 (2006).

[9] R. Savino and D. Paterna, Marangoni effect and heat pipe dry-out, Phys. Fluids **18**, 118103 (2006).

[10] R. Savino, N. di Francescantonio, R. Fortezza, and Y. Abe, Heat pipes with binary mixtures and inverse Marangoni effects for microgravity applications, Acta Astronaut. **61**, 16 (2007).

[11] R. Savino, C. Piccolo, R. Fortezza, and Y. Abe, Heat pipes with self-rewetting fluids in low-gravity conditions, Microgravity Sci. Technol. **19**, 75 (2007).
[12] N. di Francescantonio, R. Savino, and Y. Abe, New alcohol solutions for heat pipes: Marangoni effect and heat transfer enhancement, Int. J. Heat Mass Transf. **51**, 6199 (2008).
[13] R. Savino, A. Cecere, and R. Di Paola, Surface tension-driven flow in wickless heat pipes with self-rewetting fluids, Int. J. Heat Fluid Flow **30**, 380 (2009).
[14] R. Savino, R. Di Paola, A. Cecere, and R. Fortezza, Self-rewetting heat transfer fluids and nanobrines for space heat pipes, Acta Astronaut. **67**, 1030 (2010).
[15] R. Savino, D. De Cristofaro, and A. Cecere, Flow visualization and analysis of self-rewetting fluids in a model heat pipe, Int. J. Heat Mass Transf. **115**, 581 (2017).
[16] Y. Hu, T. Liu, X. Li, and S. Wang, Heat transfer enhancement of micro oscillating heat pipes with self-rewetting fluid, Int. J. Heat Mass Transf. **70**, 496 (2014).
[17] Y. Hu, S. Zhang, X. Li, and S. Wang, Heat transfer enhancement of subcooled pool boiling with self-rewetting fluid, Int. J. Heat Mass Transf. **83**, 64 (2015).
[18] S.-C. Wu, Study of self-rewetting fluid applied to loop heat pipe, Int. J. Therm. Sci. **98**, 374 (2015).
[19] A. Oron and P. Rosenau, On a nonlinear thermocapillary effect in thin liquid layers, J. Fluid Mech. **273**, 361 (1994).
[20] S. G. Slavtchev and S. P. Miladinova, Thermocapillary flow in a liquid layer at minimum in surface tension, Acta Mech. **127**, 209 (1998).
[21] W. Batson, Y. Agnon, and A. Oron, Thermocapillary modulation of self-rewetting films, J. Fluid Mech. **819**, 562 (2017).
[22] N. O. Young, J. S. Goldstein, and M. J. Block, The motion of bubbles in a vertical temperature gradient, J. Fluid Mech. **6**, 350 (1959).
[23] R. Balasubramaniam and A.-T. Chai, Thermocapillary migration of droplets: An exact solution for small Marangoni numbers, J. Colloid Interface Sci. **119**, 531 (1987).
[24] P. Ehrhard and S. H. Davis, Non-isothermal spreading of liquid drops on horizontal plates, J. Fluid Mech. **229**, 365 (1991).
[25] S. K. Wilson, The steady thermocapillary-driven motion of a large droplet in a closed tube, Phys. Fluids A **5**, 2064 (1993).
[26] S. K. Wilson, The effect of an axial temperature gradient on the steady motion of a large droplet in a tube, J. Eng. Math. **29**, 205 (1995).
[27] M. K. Smith, Thermocapillary migration of a two-dimensional liquid droplet on a solid surface, J. Fluid Mech. **294**, 209 (1995).
[28] R. Balasubramaniam and R. S. Subramanian, The migration of a drop in a uniform temperature gradient at large Marangoni numbers, Phys. Fluids **12**, 733 (2000).
[29] A. Mazouchi and G. M. Homsy, Thermocapillary migration of long bubbles in cylindrical capillary tubes, Phys. Fluids **12**, 542 (2000).
[30] A. Mazouchi and G. M. Homsy, Thermocapillary migration of long bubbles in polygonal tubes. I. Theory, Phys. Fluids **13**, 1594 (2001).
[31] E. Lajeunesse and G. M. Homsy, Thermocapillary migration of long bubbles in polygonal tubes. II. Experiments, Phys. Fluids **15**, 308 (2003).
[32] G. J. Dunn, B. R. Duffy, S. K. Wilson, and D. Holland, Quasi-steady spreading of a thin ridge of fluid with temperature-dependent surface tension on a heated or cooled substrate, Q. J. Mech. Appl. Math. **62**, 365 (2009).
[33] E. Katz, M. Haj, A. M. Leshansky, and A. Nepomnyashchy, Thermocapillary motion of a slender viscous droplet in a channel, Phys. Fluids **24**, 022102 (2012).
[34] G. Karapetsas, K. C. Sahu, and O. K. Matar, Effect of contact line dynamics on the thermocapillary motion of a droplet on an inclined plate, Langmuir **29**, 8892 (2013).
[35] G. Karapetsas, K. C. Sahu, K. Sefiane, and O. K. Matar, Thermocapillary-driven motion of a sessile drop: Effect of non-monotonic dependence of surface tension on temperature, Langmuir **30**, 4310 (2014).

[36] M. K. Tripathi, K. C. Sahu, G. Karapetsas, K. Sefiane, and O. K. Matar, Non-isothermal bubble rise: Non-monotonic dependence of surface tension on temperature, J. Fluid Mech. **763**, 82 (2015).
[37] M. E. R. Shanahan and K. Sefiane, Recalcitrant bubbles, Sci. Rep. **4**, 4727 (2014).
[38] D. Mamalis, V. Koutsos, and K. Sefiane, On the motion of a sessile drop on an incline: Effect of non-monotonic thermocapillary stresses, Appl. Phys. Lett. **109**, 231601 (2016).
[39] D. Mamalis, V. Koutsos, and K. Sefiane, Bubble rise in a non-isothermal self-rewetting fluid and the role of thermocapillarity, Int. J. Therm. Sci. **117**, 146 (2017).
[40] D. Mamalis, V. Koutsos, and K. Sefiane, Nonisothermal spreading dynamics of self-rewetting droplets, Langmuir **34**, 1916 (2018).
[41] Note that subtracting the second equation in (53) from the first yields

$$b^2\frac{dL}{dt} = Q_1|_{z=z_{\rm f}(t)} - Q_1|_{z=z_{\rm b}(t)} = Mf_{\rm M}(z_{\rm f} - z_{\rm b}) = Mf_{\rm M}L = -2bL\,\frac{db}{dt},$$

so that $d(b^2L)/dt = 0$, which recovers the volume-conservation condition $b^2L = 1$, but provides no new information.
[42] Figure 6 also illustrates that in the special case of an inviscid bubble $m = 0$ given by (60), dc/dt decreases monotonically with b_0 when $Q_{\rm b} \geqslant 0$, has a minimum value at some b_0 when $-\Delta\rho/8 < Q_{\rm b} < 0$, and increases monotonically with b_0 when $Q_{\rm b} \leqslant -\Delta\rho/8$, with $dc/dt \to \infty$ when $Q_{\rm b} > -\Delta\rho/8$, $dc/dt \to 4Q_{\rm b} = -\Delta\rho/2$ when $Q_{\rm b} = -\Delta\rho/8$, and $dc/dt \to -\infty$ when $Q_{\rm b} < -\Delta\rho/8$ in the limit $b_0 \to 0^+$.